





**Electrical transport under extreme conditions in the spin-ladder antiferromagnet TaFe<sub>1.25</sub>Te<sub>3</sub>**

Xiaofeng Xu <sup>1,\*</sup>,† Wenhao Shen,<sup>2,\*</sup> Haiyang Yang <sup>3,\*</sup> Chuanying Xi,<sup>3</sup> Junjie Bao,<sup>1</sup> Yi Liu,<sup>1</sup> Chunqiang Xu,<sup>4</sup> Tahir Murtaza <sup>1</sup>, Wen-He Jiao,<sup>1</sup> Huakun Zuo,<sup>5</sup> Ming Yang,<sup>5</sup> Junfeng Wang,<sup>5</sup> Yonghui Zhou,<sup>3</sup> Zhi Ren,<sup>6</sup> Guang-Han Cao <sup>7</sup>, Xianglin Ke,<sup>8</sup> and Zhaorong Yang<sup>3</sup>

<sup>1</sup>Key Laboratory of Quantum Precision Measurement of Zhejiang Province, Department of Applied Physics, Zhejiang University of Technology, Hangzhou 310023, China

<sup>2</sup>School of Automation, Nanjing University of Information Science & Technology, Nanjing 210044, China

<sup>3</sup>Anhui Key Laboratory of Condensed Matter Physics at Extreme Conditions, High Magnetic Field Laboratory, HFIPS, Chinese Academy of Sciences, Hefei 230031, China

<sup>4</sup>School of Physical Science and Technology, Ningbo University, Ningbo 315211, China

<sup>5</sup>Wuhan National High Magnetic Field Center, School of Physics, Huazhong University of Science and Technology, Wuhan 430074, China

<sup>6</sup>School of Science, Westlake University, Hangzhou 310064, China

<sup>7</sup>School of Physics, Zhejiang University, Hangzhou 310030, China

<sup>8</sup>Department of Physics and Astronomy, Michigan State University, East Lansing, Michigan 48824-2320, USA



(Received 11 December 2022; revised 8 February 2023; accepted 16 March 2023; published 28 March 2023)

We report the electrical transport of the layered, spin-ladder antiferromagnet TaFe<sub>1.25</sub>Te<sub>3</sub> ( $T_N \sim 167$  K) under intense magnetic field (up to 60 T) and high pressure (up to 50 GPa). In high magnetic field, TaFe<sub>1.25</sub>Te<sub>3</sub> undergoes two metamagnetic transitions, manifested in both the magnetoresistance and the Hall resistivity. Synchrotron x-ray diffraction reveals no obvious structural transition up to  $\sim 50$  GPa. However, the application of a small pressure ( $\sim 0.7$  GPa) fosters a sizable *anomalous* Hall conductivity and a negative magnetoresistance, possibly arising from the competing ferromagnetic exchange interaction in this antiferromagnet. Both the anomalous Hall conductivity and the negative magnetoresistance culminate at a pressure of  $\sim 4$  GPa. With further increase of pressure, both physical quantities diminish. The Hall coefficient and the magnetoresistance change sign above  $\sim 20$  GPa, presumably due to the cessation of ferromagnetic spin fluctuations in this high pressure regime.

DOI: [10.1103/PhysRevB.107.115156](https://doi.org/10.1103/PhysRevB.107.115156)

The study of the interplay between itinerant conduction electrons and the localized moments is one of the central themes in condensed matter physics, exemplified by the long-standing heavy-fermion problem [1,2]. This interplay may induce many novel phenomena in electrical transport, such as the logarithmic resistivity upturn, colossal magnetoresistance (CMR), and even unconventional superconductivity [3–7]. Due to this correlation, the subtle change of magnetic structure in a magnetic field, generally referred to as the metamagnetism [8], can reflect itself in the electronic transport, e.g., as a resistivity kink. A notable example is lightly doped, insulating cuprates, where a metamagnetic or spin-flop transition of the Cu moments induces an ensuing change in the hopping conductivity of the doped holes [9,10]. In turn, the itinerant electrons can also influence the magnetism through the Rudermann-Kittel-Kasuya-Yosida (RKKY) interactions [11,12]. In this regard, antiferromagnetic metals serve as an ideal playground to unveil the intricate interplay between the charge and spin degrees of freedom of a given system.

On the other hand, the discovery of iron-based high-temperature superconductors has inspired immense scientific interest in Fe-based pnictides and chalcogenides [13]. Although the iron tellurides TaFe<sub>1+y</sub>Te<sub>3</sub> were first discovered over three decades ago [14], they only garnered renewed interest in recent years, with the desire to search for high-temperature superconductivity in this series [15,16]. In spite of the fact that no superconductivity has as yet been observed in these spin-ladder compounds at ambient pressure, they constitute an intriguing platform to study novel magnetism and the interplay with conduction electrons [17]. TaFe<sub>1+y</sub>Te<sub>3</sub> possesses a layered structure with two-leg zigzag Fe ladders extending along the *b* axis and the excess amounts of Fe *y* fill the interstitials [18]. It undergoes an antiferromagnetic transition at  $T_N \sim 160$ –200 K, depending on the variation in the iron content *y* [15]. The elastic neutron scattering further revealed that the intraladder iron spins and the neighboring interstitial Fe are both coupled ferromagnetically along the FeTe chains, forming quasi-one-dimensional ferromagnetic chains, whereas their interladder coupling is antiferromagnetic essentially [17]. More interestingly, due to the existence of disordered Fe interstitials, a reentrant spin glass state was recently seen below  $T_N$ , which is responsible for the large exchange bias observed at low temperatures, arising from the

\*These authors contributed equally to this work.

†xuxiaofeng@zjut.edu.cn

synergetic effect of spin glass and antiferromagnetic orders [18]. In ARPES (angle-resolved photoemission spectroscopy) measurements, a large energy scale reconstruction of the band was observed below  $T_N$  owing to the interactions between local moments and itinerant electrons, highlighting the possible role of Hund's coupling in determining its magnetic ground state [16].

Despite these concerted efforts in revealing the mechanism of its magnetism, the charge transport properties of this layered iron telluride, in particular when coupled to the local magnetic moments, are largely unexplored [19]. In this paper, we study in detail the electrical transport of  $\text{TaFe}_{1+y}\text{Te}_3$  ( $y = 0.25$ ) in high magnetic field and under high pressure. The electrical transport in the high magnetic field reveals two metamagnetic transitions associated with the Fe moments. The pronounced change of the Hall resistivity at these metamagnetic transitions indicates its *anomalous Hall* origin [20,21]. The synchrotron x-ray diffraction, however, resolves no obvious structural transition up to  $\sim 50$  GPa. When pressurized, the resistivity kink associated with the antiferromagnetic transition is quickly suppressed and the anomalous Hall conductivity explicitly arises, accompanied with a negative magnetoresistance [22]. Both the anomalous Hall conductivity and the negative MR reach maximum values around  $\sim 4$  GPa, above which they start to diminish. Above  $\sim 20$  GPa, no anomalous Hall effect is observable, and both the normal Hall effect and the MR change sign. The intimate correlation between the anomalous Hall and the negative MR points to the same origin, i.e., the ferromagnetic coupling in this antiferromagnetic (AFM) system, which is strongest in the pressure regime of  $\sim 4$  GPa and becomes negligibly small above  $\sim 20$  GPa.

Single crystals of  $\text{TaFe}_{1.25}\text{Te}_3$  were grown by the chemical vapor transport method as described in our earlier report [18]. The crystals were checked by x-ray diffraction (XRD) and energy dispersive x-ray spectroscopy (EDS) on a PANalytical x-ray diffractometer (model EMPYREAN) and a scanning electron microscope (Hitachi S-3700N) equipped with an Oxford Instruments X-Max spectrometer, respectively. For convenience, we define two new axes  $a'$  and  $c'$  such that the  $a'$  axis (pointing along  $[101]$ ) is lying on the plane and is perpendicular to the  $b$ -axis chain direction, and the  $c'$  axis (pointing along  $[10-1]$ ) is normal to the sample top facet (see schematic inset of Fig. 1 for the orientations). The magnetization measurements were carried out on a SQUID (superconducting quantum interference device) magnetometer. The MR measurements were conducted with the four-electrode method under a pulsed magnetic field up to  $\sim 60$  T at the National High Magnetic Field Center, Wuhan. The Hall resistivity measurements were performed on a steady high magnetic field facility with fields up to  $\sim 31$  T in the High Magnetic Field Laboratory of Chinese Academy of Sciences, Hefei. The Hall voltage was antisymmetrized by changing the field polarities. High-pressure transport experiments were conducted in a nonmagnetic Be-Cu diamond anvil cell with a pair of anvil culets of  $300 \mu\text{m}$  using a homemade multifunctional measurement system [23]. A single crystal with dimensions of  $\sim 130 \times 50 \times 10 \mu\text{m}^3$  was loaded together with some ruby powder. Resistivity and Hall effect measurements under pressure were performed using the five-probe

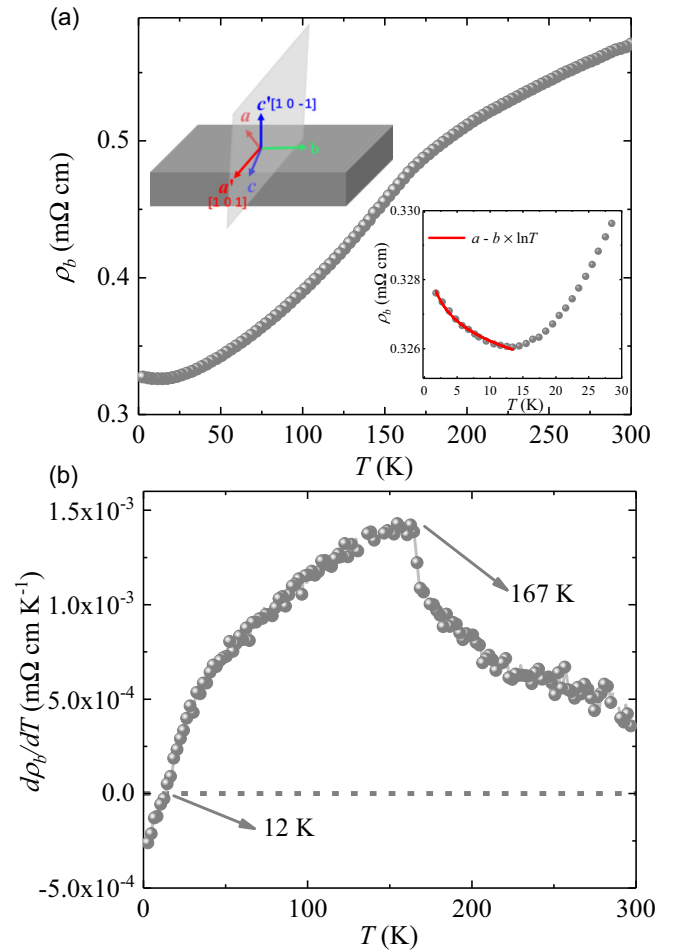


FIG. 1. (a) Zero-field intrachain resistivity from room temperature down to 1.8 K. The upper inset shows the schematic of the axes defined in the paper. The lower inset enlarges the low- $T$  resistivity upturn and the fit to the Kondo effect. (b) The derivative of the resistivity with respect to temperature  $d\rho/dT$  shows  $T_N = 167$  K and the resistivity upturn at 12 K.

method with the electric current flowing in parallel to the crystalline  $b$  axis and the magnetic field pointing along the  $c'$  axis. High-pressure angle-dispersive synchrotron XRD experiments were carried out at room temperature with  $\text{TaFe}_{1.25}\text{Te}_3$  powder crushed from single crystals, at beamline BL15U1 of the Shanghai Synchrotron Radiation Facility (SSRF) ( $\lambda = 0.6199 \text{ \AA}$ ). Pressure was calibrated by the ruby fluorescence method at room temperature for all experiments [24,25].

Figure 1 presents the zero-field in-chain resistivity  $\rho_b(T)$  from 300 K down to 1.8 K. On cooling from room temperature,  $\rho_b(T)$  shows a broad kink around  $\sim 170$  K and is metallic down to  $\sim 12$  K, followed by a well-defined, moderate upturn at low temperatures. The resistivity kink temperature, as defined using the maximum in  $d\rho/dT$  shown in the lower panel, occurs at 167 K. This corresponds to the antiferromagnetic transition temperature  $T_N$ . As demonstrated in the inset, the resistivity upturn below 12 K can be well fitted by a logarithmic scaling ( $a - b \times \ln T$ ). This logarithmic scaling suggests that the Kondo screening is responsible for the resistivity upturn

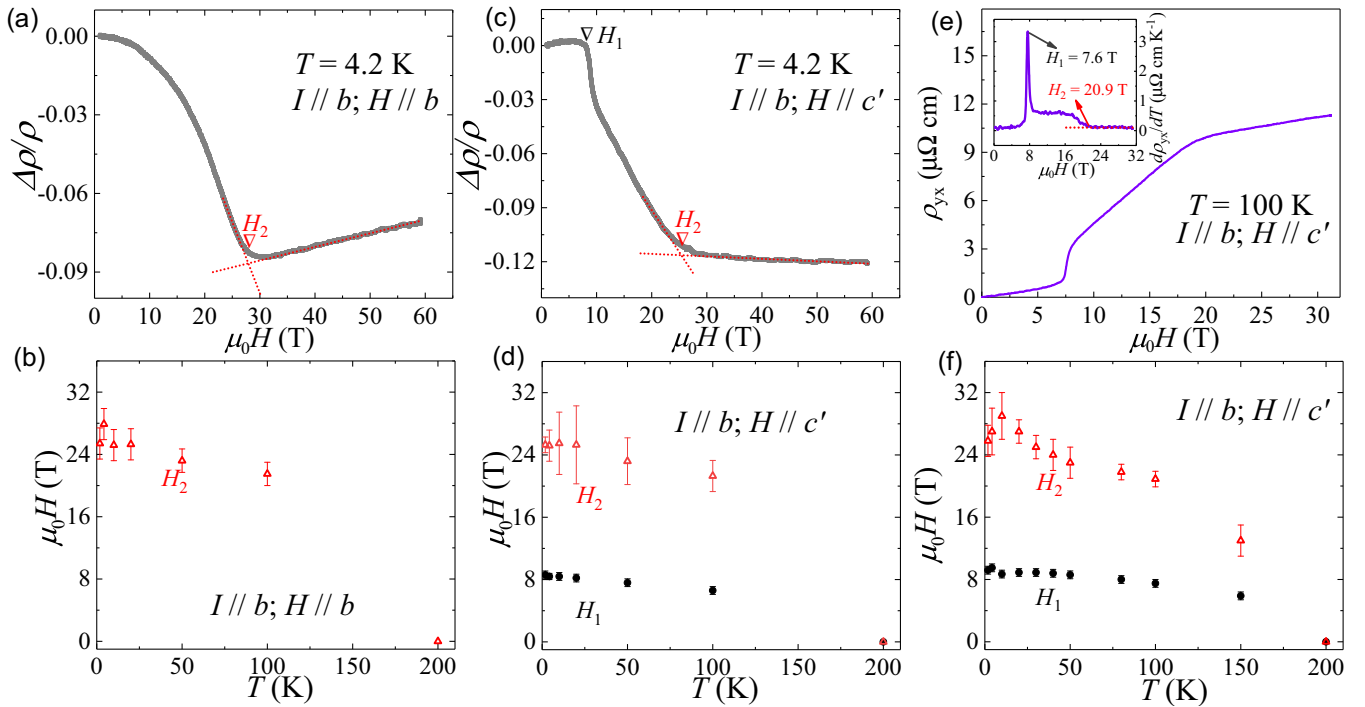


FIG. 2. The electrical transport in a high field. (a) The longitudinal intrachain MR at 4.2 K shows a metamagnetic transition at  $H_2$ . (b)  $H_2$  as a function of temperature. (c) The transverse intrachain MR at 4.2 K shows two metamagnetic transitions at  $H_1$  and  $H_2$ . (d)  $H_1$  and  $H_2$  as a function of temperature. (e) The Hall resistivity at 100 K. The inset shows  $d\rho_{yx}/dT$  to visualize the transitions at  $H_1$  and  $H_2$ . (f) The temperature variation of  $H_1$  and  $H_2$  determined from the Hall effect. In panels (b), (d), and (f), the orange color indicates the paramagnetic phase and the blue color is the antiferromagnetic state.

at low temperatures [26]. The interchain resistivity shows similar behaviors (see Fig. S1 in Ref. [27] for more details).

The intrachain longitudinal and transverse MR in the pulsed field up to  $\sim 60$  T is demonstrated in Figs. 2(a) and 2(c) for  $T = 4.2$  K, respectively. The longitudinal MR, as shown in Fig. 2(a), is negative in the whole field range measured. Clearly, there exists a kink in the MR curve around  $\sim 30$  T, marked as  $H_2$  here. Likewise, as shown in Fig. 2(c), the transverse MR is small and positive in the low fields and displays a sharp drop to negative values at  $H_1$  [15,19]. In the higher fields, the MR curve also manifests an inflection point at  $H_2$ . The MR curves in other temperatures are given in Ref. [27] (Figs. S3 and S4) and the extracted  $H_1$  and  $H_2$  values are illustrated in Figs. 2(b) and 2(d) for these two configurations, respectively. As shown, both  $H_1$  and  $H_2$  become zero above  $T_N$ , indicating that they are correlated with the Fe spins. Indeed, the magnetization measurements up to 7 T indicate that  $H_1$  is associated with the metamagnetic transition (see Fig. S2 in Ref. [27]), possibly due to the spin flop of Fe moments when  $H \parallel c'$ . So it is conceivable to associate  $H_2$  with another metamagnetic transition in the high field. In our previous study [18], we inferred that the Fe spins are predominantly aligned in the  $ac$  plane, with only a small component along the chain ( $b$  axis). Therefore, the absence of features at  $H_1$  in the  $I \parallel b$ ,  $H \parallel b$  configuration [Fig. 2(a)] can be understood. These two metamagnetic transitions at  $H_1$  and  $H_2$  are reflected in the Hall resistivity, too. As exemplified in the Hall resistivity at 100 K [Fig. 2(e); see also Fig. S5 in Ref. [27] for other temperatures],  $H_1$  and  $H_2$  manifest as kinks in  $\rho_{yx}$ , which is more clearly seen from the derivative

$d\rho_{yx}/dT$  in the inset. The  $H_1$  and  $H_2$  with their error bars extracted from the Hall effect are summarized in Fig. 2(f) and they are found to be consistent with those extracted from the MR [Figs. 2(b) and 2(d)], in terms of both the absolute values and their temperature dependence. They both become zeros above  $T_N$ .

We further performed high-pressure synchrotron XRD measurements on pulverized single crystals of  $\text{TaFe}_{1.25}\text{Te}_3$ , as shown in Fig. 3 for the two representative pressures of 3.0 and 50 GPa. The data for the other pressures are plotted in Ref. [27] (Fig. S6). In this experiment, the angle range was limited to  $2\theta = 6^\circ\text{--}24^\circ$  and the Le Bail refinement was used to analyze the underlying phases [25]. The data in the whole pressure range can be well indexed with the monoclinic  $P2_1/m$  space group. The lattice parameters are summarized in Fig. 3(c). As noted, the pressure has little bearing on the lattice parameters  $a$ ,  $b$  and  $c$ , but only varies the  $\beta$  angle smoothly. The unit-cell volume extracted from the above analysis shows a monotonic decrease with increasing pressure [Fig. 3(d)], although its slope changes evidently above  $\sim 18$  GPa. It is worth noting that, however, the good fitting of the data with the monoclinic  $P2_1/m$  space group does not necessarily exclude other space groups that may fit the data equally well. Therefore, we cannot rule out the possibility that the subtle phase transition may actually take place in this pressure regime.

The zero-field intrachain resistivity  $\rho_b(T)$  under various pressures up to  $\sim 51$  GPa is encapsulated in Fig. 4(a). As shown, the application of a pressure increases  $T_N$  to  $\sim 250$  K at 0.7–4.2 GPa, while above that the resistivity kink at

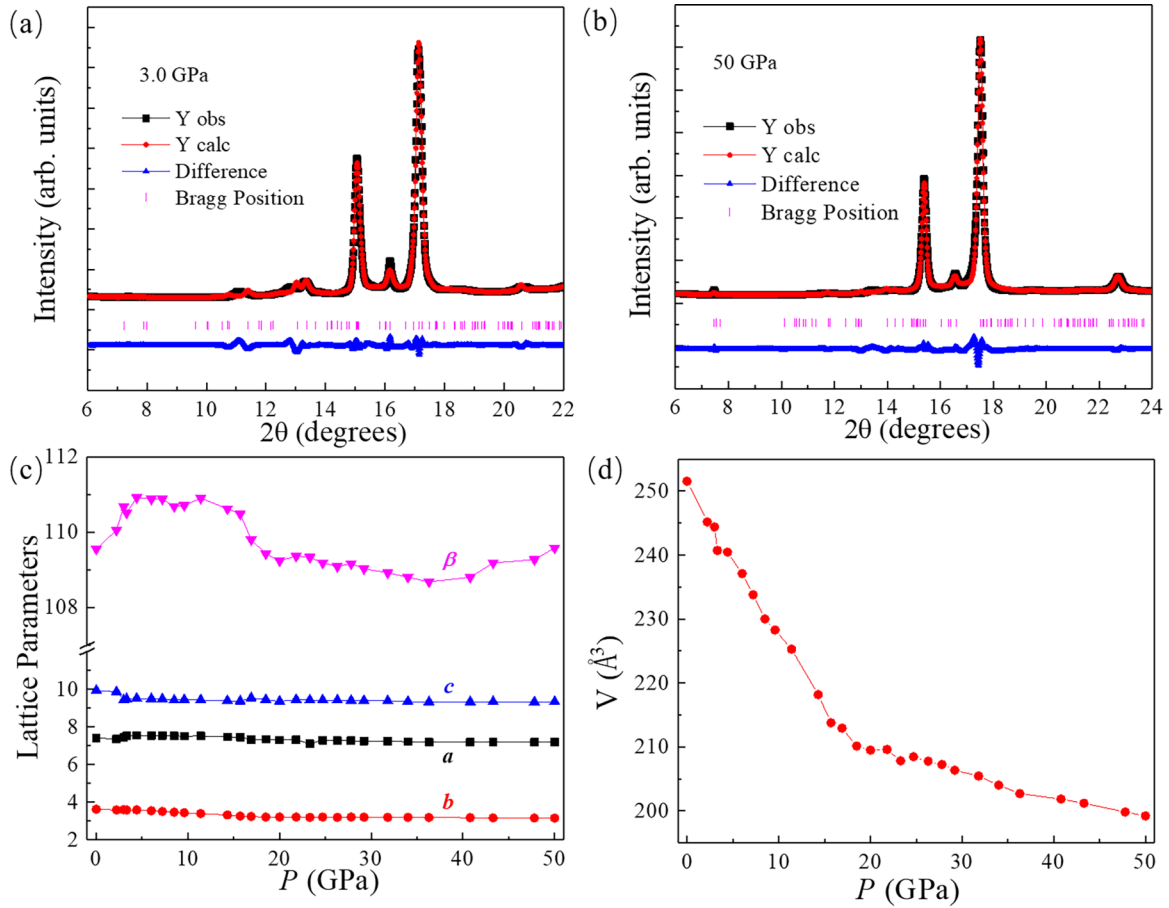


FIG. 3. (a) and (b) show the synchrotron XRD and the Le Bail refinement at 3.0 and 50 GPa, respectively. (c) The extracted lattice parameters  $a$ ,  $b$ ,  $c$ , and  $\beta$  under pressure. (d) The unit cell volumes at different pressures.

$T_N$  becomes smeared out. Overall, with increasing pressure, the resistivity is increased and no superconductivity can be observed in the pressure range studied. The MR at 5 K is negative in field under pressure below 21 GPa [Fig. 4(b)]. Above 24 GPa, it becomes overall positive [Fig. 4(c)]. Although the Hall resistivity at ambient pressure does not show any hysteresis loop in the low field associated with the anomalous Hall effect [Fig. 2(e)], it unambiguously shows the hysteresis loop under pressure, a hallmark of the anomalous Hall effect, as seen in Figs. 4(d) and 4(e). As noted, the anomalous Hall conductivity is the largest at 4.2 GPa, above which it starts to decrease. At pressure larger than 24 GPa, this anomalous Hall effect disappears altogether and the Hall resistivity becomes linear in field [Figs. 4(f) and 4(g)]. The ordinary Hall coefficient  $R_H$ , extracted from the slope of  $\rho_{yx}$  above the hysteresis, is plotted as a function of pressure in Fig. 4(h). As shown,  $R_H$  also changes sign above  $\sim 20$  GPa. The contour plot of the intrachain resistivity under different pressures, along with the MR and the anomalous Hall conductivity  $\sigma_{xy}^A$  ( $= -\sigma_{yx}^A = \frac{\rho_{yx}^A}{(\rho_{xx})^2 + (\rho_{yx}^A)^2}$ ) at 5 K, is presented in Fig. 4(i). Remarkably, both the negative MR and  $\sigma_{xy}^A$  reach a maximum value at  $\sim 4.2$  GPa. With further increasing pressure, they start to decrease; above  $\sim 20$  GPa, the anomalous Hall effect disappears and the MR evolves from negative to positive.

A plausible scenario for the anomalous Hall effect and the negative MR seen in this AFM system under pressure is as follows. Although the antiferromagnetic exchange interactions dominate in this iron telluride, FM coupling also exists, evidenced from the spin glass state at low temperatures arising from the competition between FM and AFM interactions [18]. The FM fluctuations in this system are not surprising given that the Fe spins are ferromagnetically coupled along the chains [17]. Under pressure, the FM interactions (possibly also the AFM interactions) are further enhanced, leading to pronounced anomalous Hall effect and the large negative MR, both of which attain the maximum at  $\sim 4$  GPa. With further increasing pressure, the FM coupling starts to decline. Above  $\sim 20$  GPa, both the FM and AFM are weak and the positive MR and the ordinary Hall effect take over.

To summarize, we have investigated the electrical transport properties of the spin-ladder antiferromagnet  $\text{TaFe}_{1.25}\text{Te}_3$  in a high magnetic field and under high pressure. A large negative MR is observed in both the longitudinal and transverse fields, which may be attributed to the suppression of the spin fluctuations in field. Two metamagnetic transitions are resolved in its MR and Hall responses. Although the pressure induces no structural transition up to  $\sim 50$  GPa, both the anomalous Hall effect and the negative MR reach maximum values at  $\sim 4$  GPa, suggestive of the strongest FM fluctuations in this AFM

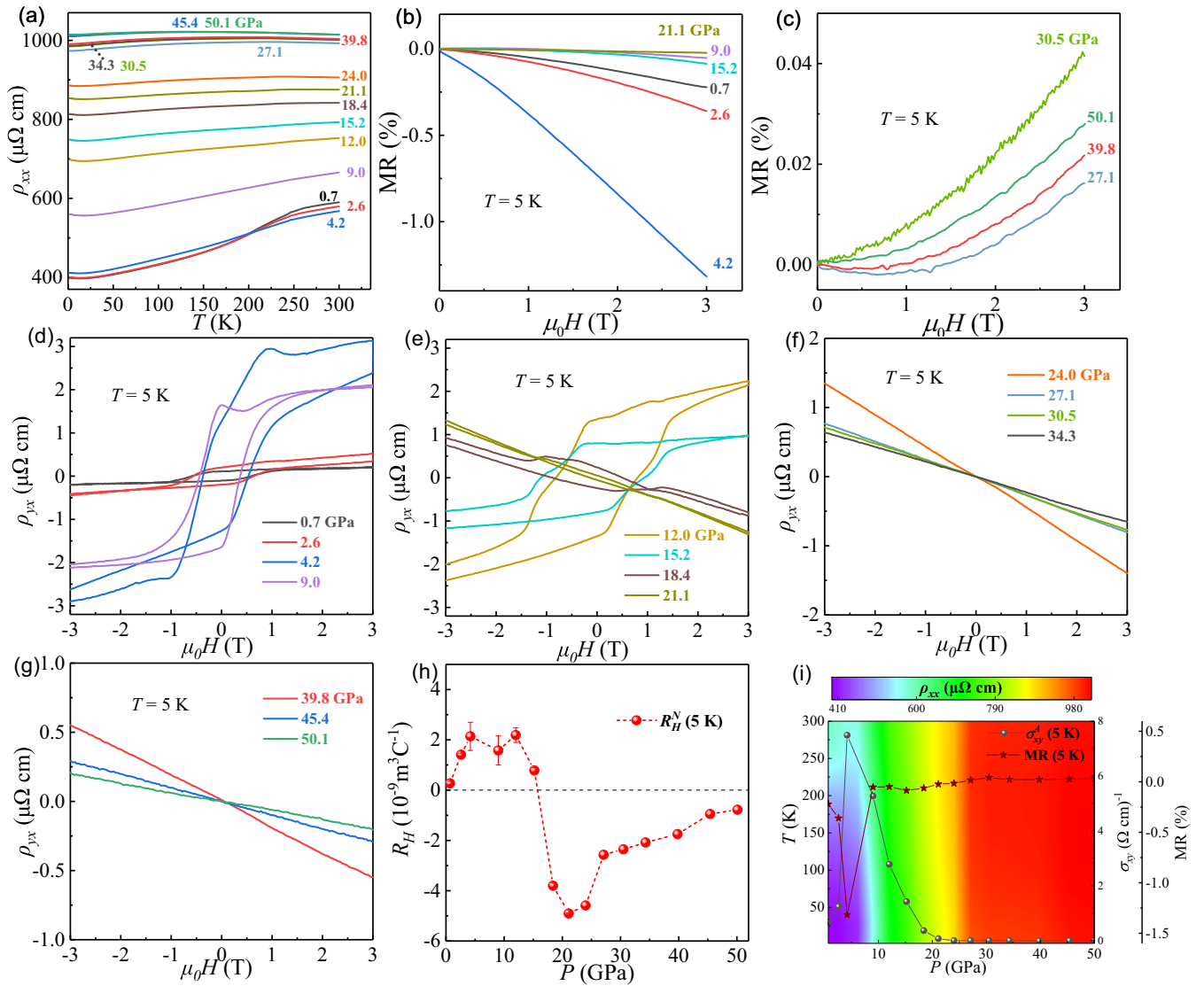


FIG. 4. (a) The zero-field resistivity under various pressures. (b) and (c) show the MR in the low field at different pressures ( $T = 5$  K). (d)–(g) The Hall resistivity at different pressures ( $T = 5$  K). (h) The ordinary Hall coefficient as a function of pressure. (i) The contour color plot of resistivity under different pressures, overlaid with the curves of the anomalous Hall conductivity and the MR at 5 K.

system in this pressure regime. These findings thus raise an exciting prospect to investigate how the itinerant electrons can be coupled with the magnetism to ultimately introduce novel transport properties.

#### ACKNOWLEDGMENTS

The authors would like to thank Nigel Hussey, Michael Smidman, Xin Lu, Yang Liu, Dong Qian, and Xiangang Wan

for valuable discussions. This research was supported by National Natural Science Foundation of China under Grants No. 12274369, No. 11974061, No. 12074135, and No. 12004122, by the Zhejiang Provincial Natural Science Foundation of China (Grant No. LZ23A040002), and by the Users with Excellence Project of Hefei Science Center CAS, 2021HSC-UE007. The synchrotron XRD under pressure was performed in Beamline BL15U1 of the Shanghai Synchrotron Radiation Facility (SSRF).

- [1] P. Coleman, *Introduction to Many-Body Physics* (Cambridge University Press, 2015).  
 [2] G. R. Stewart, Heavy-fermion systems, *Rev. Mod. Phys.* **56**, 755 (1984).

- [3] Y. Tokura, Critical features of colossal magnetoresistive manganites, *Rep. Prog. Phys.* **69**, 797 (2006).  
 [4] F. Steglich, Heavy-fermion superconductivity in the Kondo-lattice system CeCu<sub>2</sub>Si<sub>2</sub>, *J. Phys.: Conf. Ser.* **400**, 022111 (2012).



- [5] P. W. Phillips, N. E. Hussey, and P. Abbamonte, Stranger than metals, *Science* **377**, eabh4273 (2022).
- [6] L. Zeng, X. Hu, S. Guo, G. Lin, J. Song, K. Li, Y. He, Y. Huang, C. Zhang, P. Yu, J. Ma, D.-X. Yao, and H. X. Luo, Ta<sub>4</sub>CoSi: A tantalum-rich superconductor with a honeycomb network structure, *Phys. Rev. B* **106**, 134501 (2022).
- [7] J. A. T. Barker, D. Singh, A. Thamizhavel, A. D. Hillier, M. R. Lees, G. Balakrishnan, D. M. Paul, and R. P. Singh, Unconventional Superconductivity in La<sub>7</sub>Ir<sub>3</sub> Revealed by Muon Spin Relaxation: Introducing a New Family of Noncentrosymmetric Superconductor That Breaks Time-Reversal Symmetry, *Phys. Rev. Lett.* **115**, 267001 (2015).
- [8] E. Stryjewski and N. Giordano, Metamagnetism, *Adv. Phys.* **26**, 487 (1977).
- [9] T. Thio, T. R. Thurston, N. W. Preyer, P. J. Picone, M. A. Kastner, H. P. Jenssen, D. R. Gabbe, C. Y. Chen, R. J. Birgeneau, and A. Aharony, Antisymmetric exchange and its influence on the magnetic structure and conductivity of La<sub>2</sub>CuO<sub>4</sub>, *Phys. Rev. B* **38**, 905(R) (1988).
- [10] A. N. Lavrov, H. J. Kang, Y. Kurita, T. Suzuki, S. Komiya, J. W. Lynn, S.-H. Lee, P. C. Dai, and Y. Ando, Spin-Flop Transition and the Anisotropic Magnetoresistance of Pr<sub>1.3-x</sub>La<sub>0.7</sub>Ce<sub>x</sub>CuO<sub>4</sub>: Unexpectedly Strong Spin-Charge Coupling in the Electron-Doped Cuprates, *Phys. Rev. Lett.* **92**, 227003 (2004).
- [11] S. Blundell, *Magnetism in Condensed Matter* (Oxford University Press, Oxford, 2001).
- [12] X. Xu, A. Carrington, A. I. Coldea, A. Enayati-Rad, A. Narduzzo, S. Hori, and N. E. Hussey, Dimensionality-driven spin-flop transition in quasi-one-dimensional PrBa<sub>2</sub>Cu<sub>4</sub>O<sub>8</sub>, *Phys. Rev. B* **81**, 224435 (2010).
- [13] G. R. Stewart, Superconductivity in iron compounds, *Rev. Mod. Phys.* **83**, 1589 (2011).
- [14] M. E. Badding, J. Li, F. J. Disalvo, W. Zhou, and P. P. Edwards, Characterization of TaFe<sub>1.25</sub>Te<sub>3</sub>, a new layered telluride with an unusual metal network structure, *J. Solid State Chem.* **100**, 313 (1992).
- [15] R. H. Liu, M. Zhang, P. Cheng, Y. J. Yan, Z. J. Xiang, J. J. Ying, X. F. Wang, A. F. Wang, G. J. Ye, X. G. Luo, and X. H. Chen, Spin-density-wave transition of Fe1 zigzag chains and metamagnetic transition of Fe<sub>2</sub> in TaFe<sub>1+y</sub>Te<sub>3</sub>, *Phys. Rev. B* **84**, 184432 (2011).
- [16] M. Xu, L. Wang, R. Peng, Q. Ge, F. Chen, Z. Ye, Y. Zhang, S. Chen, M. Xia, R. Liu, M. Arita, K. Shimada, H. Namatame, M. Taniguchi, M. Matsunami, S. Kimura, M. Shi, X. Chen, W. Yin, W. Ku *et al.*, Electronic structure reconstruction across the antiferromagnetic transition in TaFe<sub>1.23</sub>Te<sub>3</sub> spin ladder, *Chin. Phys. Lett.* **32**, 027401 (2015).
- [17] X. Ke, B. Qian, H. Cao, J. Hu, G. C. Wang, and Z. Q. Mao, Magnetic structure of quasi-one-dimensional antiferromagnetic TaFe<sub>1+y</sub>Te<sub>3</sub>, *Phys. Rev. B* **85**, 214404 (2012).
- [18] Y. Liu, J. J. Bao, C. Q. Xu, W. H. Jiao, H. Zhang, L. C. Xu, Z. Zhu, H. Y. Yang, Y. Zhou, Z. Ren, P. K. Biswas, S. K. Ghosh, Z. Yang, X. Ke, G. H. Cao, and X. Xu, Coupling between antiferromagnetic and spin-glass orders in the quasi-one-dimensional iron telluride TaFe<sub>1+x</sub>Te<sub>3</sub> ( $x = 0.25$ ), *Phys. Rev. B* **104**, 104418 (2021).
- [19] R. Roy Chowdhury, S. DuttaGupta, C. Patra, A. Kataria, S. Fukami, and R. P. Singh, Anisotropic magnetotransport in the layered antiferromagnet TaFe<sub>1.25</sub>Te<sub>3</sub>, *Phys. Rev. Mater.* **6**, 084408 (2022).
- [20] N. Nagaosa, J. Sinova, S. Onoda, A. H. MacDonald, and N. P. Ong, Anomalous Hall effect, *Rev. Mod. Phys.* **82**, 1539 (2010).
- [21] D. Xiao, M.-C. Chang, and Q. Niu, Berry phase effects on electronic properties, *Rev. Mod. Phys.* **82**, 1959 (2010).
- [22] W. Zhou, C. Q. Xu, B. Li, R. Sankar, F. M. Zhang, B. Qian, C. Cao, J. H. Dai, J. Lu, W. X. Jiang, D. Qian, and X. Xu, Kondo behavior and metamagnetic phase transition in the heavy-Fermion compound CeBi<sub>2</sub>, *Phys. Rev. B* **97**, 195120 (2018).
- [23] H. Y. Yang, Y. H. Zhou, L. Y. Li, Z. Chen, Z. Y. Zhang, S. Y. Wang, J. Wang, X. L. Chen, C. An, Y. Zhou, M. Zhang, R. R. Zhang, X. D. Zhu, L. L. Zhang, X. P. Yang, and Z. R. Yang, Pressure-induced superconductivity in quasi-one-dimensional semimetal Ta<sub>2</sub>PdSe<sub>6</sub>, *Phys. Rev. Mater.* **6**, 084803 (2022).
- [24] H. K. Mao, J. Xu, and P. M. Bell, Calibration of the Ruby pressure gauge to 800 kbar under quasi-hydrostatic conditions, *J. Geophys. Res.* **91**, 4673 (1986).
- [25] T. Murtaza, H. Yang, J. Feng, Y. Shen, Y. Ge, Y. Liu, C. Xu, W. Jiao, Y. Lv, C. J. Ridley, C. L. Bull, P. K. Biswas, R. Sankar, W. Zhou, B. Qian, X. Jiang, Z. Feng, Y. Zhou, Z. Zhu, Z. Yang *et al.*, Cascade of pressure-driven phase transitions in the topological nodal-line superconductor PbTaSe<sub>2</sub>, *Phys. Rev. B* **106**, L060501 (2022).
- [26] Z. F. Weng, M. Smidman, L. Jiao, X. Lu, and H. Q. Yuan, Multiple quantum phase transitions and superconductivity in Ce-based heavy fermions, *Rep. Prog. Phys.* **79**, 094503 (2016).
- [27] See Supplemental Material at <http://link.aps.org/supplemental/10.1103/PhysRevB.107.115156> for more measurements on the interchain resistivity, high-field magnetotransport, and the synchrotron XRD under pressure.